Inorganic Chemistry
Article

Inorg. Chem. **2010**, *49*, 6005–6012 **6005**
DOI: 10.1021/ic100646e

Four New Dysprosium and Neodymium Octamolybdate Hydrates: Assembly of $RE_2(Mo_8O_{27})$ Sheets and Topotactic Transformations

Xiaojun Kuang and Ivana R. Evans*

Department of Chemistry, University of Durham, Science Site, South Road, Durham DH1 3LE, England, United Kingdom

Received April 6, 2010

Four new Dy and Nd hydrated octamolybdate materials have been prepared: $[Dy_2(H_2O)_{12}](Mo_8O_{27})\cdot 8H_2O$, $[Dy_2(H_2O)_6](Mo_8O_{27})$, $[Nd_2(H_2O)_{12}](Mo_8O_{27})\cdot 6H_2O$, and $[Nd_2(H_2O)_6]Mo_8O_{27}\cdot 3H_2O$. They adopt one known and three new structure types, which we have determined ab initio from powder X-ray diffraction data. The four compounds contain the same basic structural building block, in the form of $RE_2Mo_8O_{27}$ (RE = Dy, Nd) chains, which are arranged differently for the two rare earths in the fully hydrated precursor materials. $[Dy_2(H_2O)_{12}](Mo_8O_{27})\cdot 8H_2O$ comprises isolated $Dy_2Mo_8O_{27}$ chains assembled in a zigzag manner along the *a* axis with interspersed crystallized water molecules, which differs from the parallel arrangements of isolated $Nd_2Mo_8O_{27}$ chains in $[Nd_2(H_2O)_{12}](Mo_8O_{27})\cdot 6H_2O$. Partial dehydration of the two precursors leads to new phases $[Dy_2(H_2O)_6](Mo_8O_{27})$ and $[Nd_2(H_2O)_6]Mo_8O_{27}\cdot 3H_2O$, respectively, prior to complete dehydration, which leads to initially amorphous and eventually crystalline rare-earth molybdenum mixed metal oxides. Both initial transformations occur topotactically. Partial dehydration of the Dy phase condenses the assembly of the $Dy_2Mo_8O_{27}$ chains principally along the *a* axis, leading to a 3-dimensional (3D) framework, with each Dy bridging two $(Mo_8O_{27})^{6-}$ sheets in the product. The partial dehydration of the Nd precursor condenses the assembly of $Nd_2Mo_8O_{27}$ chains along the [110] axis, leading to a 3D framework where each Nd bridges three $(Mo_8O_{27})^{6-}$ units. Both new dysprosium octamolybdates adopt noncentrosymmetric polar structures in space group $P2_1$ and are second harmonic generation (SHG) active.

Introduction

Rare-earth-containing molybdates display a variety of interesting properties including catalytic activity, negative thermal expansion, ferroelectricity and ferroelasticity, oxide ion conductivity, and complex structural behavior.[1−8] Polyoxometalate materials have also received significant attention owing to their applications in biology and medicine and catalysis, as photoluminescencent and nonlinear optical materials, as well as precursors for oxide materials.[9,10] There is also considerable interest in mixed-valence polyoxomolybdates,[11−13] which can be used as building units for new structural topologies and in the development of new giant inorganic molecules materials for molecular uptake and storage and nanoassembly, with novel magnetic and conducting properties.

Intramolecular energy transfer in europium octamolybdate hydrate $[Eu_2(H_2O)_{12}](Mo_8O_{27})\cdot 6H_2O$ and its samarium analogue have been investigated in the context of their application in electroluminescent devices.[14−16] The structures of these materials contain the $(Mo_8O_{27})_n^{6-}$ motifs found in ammonium octamolybdate $(NH_4)_6(Mo_8O_{27})\cdot 4H_2O$.[17] The $(Mo_8O_{27})^{6-}$ groups, formed by edge-sharing MoO_6 octahedra, are linked by shared corners into $(Mo_8O_{27})_n^{6-}$ polyhedral sheets.

*To whom correspondence should be addressed. E-mail: ivana.radosavljevic@durham.ac.uk.

(1) Agarwal, D. D.; Madhok, K. L.; Goswami, H. S. *React. Kinet. Catal. Lett.* **1994**, *52*, 225.
(2) De Smet, F.; Devillers, M.; Poleunis, C.; Bertrand, P. *J. Chem. Soc., Faraday Trans.* **1998**, *94*, 941.
(3) De Smet, F.; Ruiz, P.; Delmon, B.; Devillers, M. *J. Phys. Chem. B* **2001**, *105*, 12355.
(4) Evans, J. S. O. *J. Chem. Soc., Dalton Trans.* **1999**, 3317.
(5) Jeitschko, W *Acta Crystallogr., Sect. B* **1972**, *28*, 60.
(6) Abrahams, S. C.; Svensson, C.; Bernstein, J. L. *J. Chem. Phys.* **1980**, *72*, 4278.
(7) Lacorre, P.; Goutenoire, F.; Bohnke, O.; Retoux, R.; Laligant, Y. *Nature* **2000**, *404*, 856.
(8) Evans, I. R.; Howard, J. A. K.; Evans, J. S. O. *Chem. Mater.* **2005**, *17*, 4074.
(9) Katsoulis, D. E. *Chem. Rev.* **1998**, *98*, 359.
(10) Coronado, E.; Gomez-Garcia, C. J. *Chem. Rev.* **1998**, *98*, 273.
(11) Long, D. L.; Burkholder, E.; Cronin, L. *Chem. Soc. Rev.* **2007**, *36*, 105.
(12) Muller, A.; Krickemeyer, E.; Bogge, H.; Schmidtmann, M.; Peters, F. *Angew. Chem., Int. Ed.* **1998**, *37*, 3360.
(13) Muller, A.; Peters, F.; Pope, M. T.; Gatteschi, D. *Chem. Rev.* **1998**, *98*, 239.
(14) Yamase, T.; Naruke, H. *Coord. Chem. Rev.* **1991**, *111*, 83.
(15) Yamase, T.; Naruke, H. *J. Chem. Soc., Dalton Trans.* **1991**, 285.
(16) Yamase, T.; Ozeki, T.; Kawashima, I. *Acta Crystallogr., Sect. C* **1995**, *51*, 545.
(17) Boschen, I.; Buss, B.; Krebs, B. *Acta Crystallogr., Sect. B* **1974**, *30*, 48.

Published on Web 06/03/2010

The Eu and Sm materials are isostructural and adopt centrosymmetric triclinic ($P\bar{1}$) structures, which comprise isolated $RE_2Mo_8O_{27}$ sheets packed in a parallel manner, with interspersed crystallized water molecules. These materials have also been used as precursors to form single crystals of a number of mixed metal oxides, namely, those with formulas $RE_4Mo_7O_{27}$, $RE_6Mo_{10}O_{39}$, $RE_6Mo_{12}O_{45}$, and $RE_2Mo_5O_{18}$. However, in all of these cases, only single crystals were formed from partially fused solids, through routes which involved melting and quenching the precursor, characterized by poor reproducibility and a pronounced dependence of the synthetic outcomes on the precise thermal history and reaction vessel history.[18−21]

In this study, we report four new Dy and Nd molybdate materials: highly hydrated $[Dy_2(H_2O)_{12}](Mo_8O_{27})\cdot 8H_2O$ and its partially dehydrated product $[Dy_2(H_2O)_6](Mo_8O_{27})$ and highly hydrated $[Nd_2(H_2O)_{12}](Mo_8O_{27})\cdot 6H_2O$ and its partially dehydrated product $[Nd_2(H_2O)_6]Mo_8O_{27}\cdot 3H_2O$. The four compounds crystallize in one known and three new structure types, which we have solved ab initio from laboratory powder X-ray diffraction data. The partial dehydration of both highly hydrated rare-earth octamolybdates topotactically condenses the isolated $RE_2Mo_8O_{27}$ chains into three-dimensionally linked framework structures, resulting in channels along the $(Mo_8O_{27})^{6-}$ chain direction in the products obtained. The thermal decompositions of dysprosium and neodymium precursors were investigated by in situ variable temperature X-ray diffraction, and the compounds were additionally characterized by thermal analysis and second harmonic generation (SHG) measurements. Both new dysprosium octamolybdates adopt crystal structures characterized by a zigzag assembly of $Dy_2Mo_8O_{27}$ building units, in the noncentrosymmetric polar space group $P2_1$.

Experimental section

Synthesis. Polycrystalline $[Dy_2(H_2O)_{12}](Mo_8O_{27})\cdot 8H_2O$ was synthesized following the method reported for the Eu hexahydrate by Yamase and Naruke.[15] A total of 1.2497 g (5.24×10^{-3} mol) of K_2MoO_4 (Alfa Aesar, 99.9%) was dissolved in 800 mL of deionized water. Hydrochloric acid (Fisher) was used to acidify the solution to pH = 3, before adding 0.5754 g (1.31×10^{-3} mol) of $Dy(NO_3)_3\cdot 5H_2O$ (Aldrich, 99.9%), with continuous stirring for 2 h. The solution was kept still in a beaker at ambient temperature for 7 days, and a white $[Dy_2(H_2O)_{12}](Mo_8O_{27})\cdot 8H_2O$ powder was precipitated from the solution. The precipitate was collected by filtration, washed with water, and dried overnight in the air. Partial dehydration of bulk $[Dy_2(H_2O)_{12}](Mo_8O_{27})\cdot 8H_2O$ was performed by heating at 100 °C for 3 h with a 1 °C/min heating rate and a 2 °C/min cooling rate, which resulted in a partially dehydrated phase $[Dy_2(H_2O)_6](Mo_8O_{27})$. The synthesis of $[Nd_2(H_2O)_{12}](Mo_8O_{27})\cdot 6H_2O$ was carried out using a similar procedure, for which 1.2803 g (5.37×10^{-3} mol) of K_2MoO_4, 0.5892 g (1.34×10^{-3} mol) of $Nd(NO_3)_3\cdot 6H_2O$ (Aldrich, 99.9%), and 750 mL of deionized water were used. A pink powder of $[Nd_2(H_2O)_{12}](Mo_8O_{27})\cdot 6H_2O$ was precipitated from the solution. A bulk sample of partially dehydrated $[Nd_2(H_2O)_6]Mo_8O_{27}\cdot 3H_2O$ was prepared by heating the $[Nd_2(H_2O)_{12}](Mo_8O_{27})\cdot 6H_2O$ precursor at 80 °C for 4.5 h using a 1 °C/min heating rate and a 2 °C/min cooling rate.

Characterization. The water content of all samples was determined by thermogravimetric analysis (TGA) in the air from ambient temperature to 700 °C, with a heating rate of 5 °C/min, on a Perkin-Elmer thermogravimetry Pyris 1 instrument. SHG measurements were conducted using a modified Kurtz-NLO system with a 1064 nm light source. The 532 nm SHG was collected in reflection and detected using a photomultiplier tube. A 532 nm narrow-bandpass interference filter was attached to the tube in order to only detect SHG light.[22] Variable temperature powder X-ray diffraction (VT XRD) was performed from ambient temperature to 800 °C on a Bruker AXS D8 Advance diffractometer using Cu Kα1 radiation, equipped with a Vantec detector and an Anton Paar HTK1200 high-temperature attachment. The data collections were performed over a 2θ range of 5−90°, with an acquisition time of 2.3 h at each temperature. The phase assignments at different temperatures were carried out using the JCPDS database in the EVA software, as well as by performing multiple-phase Rietveld refinement on the VT XRD data. High quality powder XRD data for ab initio structure solutions and Rietveld refinements were collected at ambient temperature on a Bruker D8 Advance instrument with a LynxEye detector, in a range from 5 to 90° 2θ, using a step size of 0.017° and a step time of 8−10 s.

Structural Analysis. The laboratory powder X-ray patterns were indexed using Topas Academic software.[23] The crystal structures of the three new materials were solved by direct methods implemented in the program EXPO,[24] which gave the rare earth and molybdenum cation sites, revealing a similar RE_2Mo_8 unit to that observed in the europium octamolybdate. The initial structural models were therefore constructed by adding the oxygen sites into $(Mo_8O_{27})^{6-}$ groups according to the positions in the europium octamolybdate and placing the crystal water oxygen sites randomly between the $RE_2Mo_8O_{27}$ units and refining them using Topas Academic software.[23] Because of the low scattering contribution of oxygen to the XRD data, a minimum interoxygen distance of 2.4 Å was applied during the refinement to avoid close contacts between oxygen atoms; Mo−O bond length restraints (1.6−2.5 Å) were also applied to the MoO_6 octahedra to get chemically sensible environments for Mo^{6+}. The zero point, a background function, and a peak-shape profile function coefficient were also refined for each pattern. The bond valence sums (BVSs) were calculated using Brown and Altermatt's method[25] using the SPuDS program.[26] The crystallographic data, refinement details, and selected average bond lengths for the four compounds are summarized in Table 1.

Results and Discussion

Structure of $[Dy_2(H_2O)_{12}](Mo_8O_{27})\cdot 8H_2O$. $[Dy_2(H_2O)_{12}](Mo_8O_{27})\cdot 8H_2O$ adopts a new structure type in polar space group $P2_1$ (Figure 1a,b). The asymmetric unit consists of two Dy, eight Mo, and 47 O atoms. The noncentrosymmetric space group is consistent with the SHG measurement result, which shows that this material is SGH active with an efficiency 5 times that of α-SiO_2.

The final refined structural parameters for $[Dy_2(H_2O)_{12}](Mo_8O_{27})\cdot 8H_2O$ are listed in Table S1 in the Supporting Information, while Dy−O and Mo−O bond lengths are listed in Table 2. The final refinement agreement

(18) Naruke, H.; Yamase, T. *J. Solid State Chem.* **2001**, *161*, 85.
(19) Naruke, H.; Yamase, T. *Inorg. Chem.* **2002**, *41*, 6514.
(20) Naruke, H.; Yamase, T. *J. Solid State Chem.* **2003**, 173.
(21) Naruke, H.; Yamase, T. *J. Solid State Chem.* **2005**, *178*, 702.
(22) Ok, K. M.; Chi, E. O.; Halasyamani, P. S. *Chem. Soc. Rev.* **2006**, *35*, 710.
(23) Coelho, A. A. *TOPAS Academic*, v4; Coelho Software: Brisbane, Australia, **2005**.
(24) Altomare, A.; Burla, M. C.; Camalli, M.; Carrozzini, B.; Cascarano, G. L.; Giacovazzo, C.; Guagliardi, A.; Moliterni, A. G. G.; Polidori, G.; Rizzi, R. *J. Appl. Crystallogr.* **1999**, *32*, 339.
(25) Brown, I. D.; Altermatt, D. *Acta Crystallogr., Sect. B* **1985**, *41*, 244.
(26) Lufaso, M. W.; Woodward, P. M. *Acta Crystallogr., Sect. B* **2001**, *57*, 725.

Table 1. Water Content from TGA, Crystallographic Data, Refinement Details, and Selected Bond Lengths for Dy and Nd Octamolybdates

compound	$[Dy_2(H_2O)_{12}](Mo_8O_{27})\cdot 8H_2O$	$[Dy_2(H_2O)_6]Mo_8O_{27}$	$[Nd_2(H_2O)_{12}](Mo_8O_{27})\cdot 6H_2O$	$[Nd_2(H_2O)_6](Mo_8O_{27})\cdot 3H_2O$
H_2O (per $RE_2Mo_8O_{27}$)	20.0(1)	6.2(2)	18.4(1)	8.7(1)
color	white	light yellow	pink	gray
space group	$P2_1$	$P2_1$	$P\bar{1}$	$P\bar{1}$
Z	2	2	1	1
a (Å)	20.7738(4)	14.1242(5)	10.1663(3)	8.9907(4)
b (Å)	10.2203(2)	10.1306(4)	12.0371(3)	10.3378(5)
c (Å)	9.3114(2)	9.2981(5)	9.3791(3)	9.2857(5)
α (deg)	90	90	122.544(2)	112.853(5)
β (deg)	83.904(2)	89.852(6)	90.223(2)	91.505(5)
γ (deg)	90	90	98.236(2)	111.768(4)
V (Å^3)	1965.77(8)	1330.4(1)	953.03(5)	723.83(8)
ρ_{calc} (g/cm^3)	3.12	4.05	3.09	3.74
$R_{wp}/R_p/R_B$ (%)	6.50/5.07/2.69	1.52/1.08/0.46	3.96/2.66/1.89	5.73/4.39/1.90
RE−O (Å)	2.29−2.59	2.22−2.51	2.41−2.68	2.40−2.49
$(RE-O)_{average}$ (Å)	2.42	2.41	2.50	2.45
Mo−$O_{terminal}$ (Å)	1.67−1.80	1.65−1.75	1.69−1.77	1.65−1.81
$(Mo-O_{terminal})_{average}$ (Å)	1.72	1.71	1.74	1.72

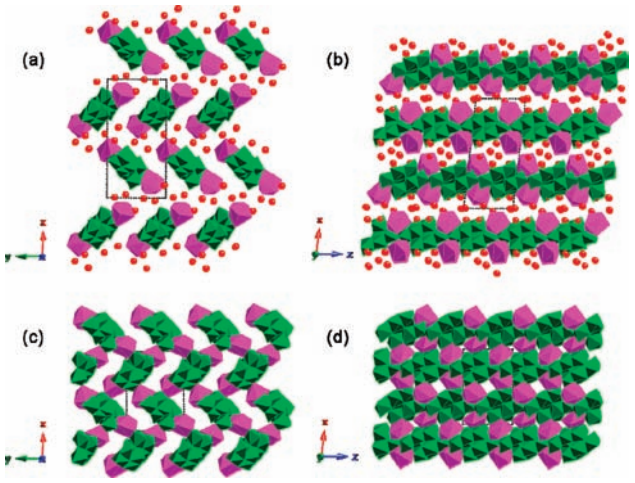

Figure 1. Two views of the crystal structure of $[Dy_2(H_2O)_{12}](Mo_8O_{27})\cdot 8H_2O$, (a) along [001] and (b) along [010], and the crystal structure of the partially dehydrated product $[Dy_2(H_2O)_6](Mo_8O_{27})$, (c) along [001] and (d) along [010]. The red spheres represent the water oxygen atoms not coordinated to Dy (in pink polyhedra); MoO_6 octahedra are shown in green.

factors obtained were $R_p = 5.07\%$ and $R_{wp} = 6.50\%$, and the Rietveld plot is shown in Figure 2.

The coordination geometry of the Dy cations in $[Dy_2(H_2O)_{12}](Mo_8O_{27})\cdot 8H_2O$ is similar to that of Eu in $[Eu_2(H_2O)_{12}](Mo_8O_{27}))\cdot 6H_2O$, with three oxygen atoms from the $(Mo_8O_{27})^{6-}$ units and six oxygen atoms from water bonded to Dy, leading to a coordination number of 9 and a tricapped trigonal prismatic environment. The calculated BVSs for the two unique Dy^{3+} cations are 2.95 and 2.98, while for the six independent Mo^{6+} sites, they vary from 5.78 to 6.35. The $Dy_2Mo_8O_{27}$ units are assembled in a zigzag (herringbone) manner along the a axis (Figure 1a), in contrast to the parallel arrangement previously found in $[Eu_2(H_2O)_{12}](Mo_8O_{27})\cdot 6H_2O$. The zigzag-type assembly of $(Mo_8O_{27})^{6-}$ in $[Dy_2(H_2O)_{12}](Mo_8O_{27})\cdot 8H_2O$ is similar to that in $(NH_4)_6(Mo_8O_{27})\cdot 4H_2O$, which, however, adopts a centrosymmetric $P2_1/c$ structure. Different packing arrangements of polyoxoanion units (parallel vs zigzag), dependent on the nature of the rare-earth cation, have previously been reported in Nd, Eu, and Yb compounds containing the $RE_n(SiW_{11}O_{39})$ polyoxoanion building blocks.[27]

Table 2. Bond Lengths and Bond Valence Sums of Dy^{3+} and Mo^{6+} in $[Dy_2(H_2O)_{12}](Mo_8O_{27})\cdot 8H_2O$

bond	bond length (Å)	bond	bond length (Å)
Dy1−O45	2.29(4)	Mo4−O23	1.69(4)
Dy1−O7	2.32(4)	Mo4−O36	1.70(5)
Dy1−O39	2.34(4)	Mo4−O22	1.87(3)
Dy1−O34	2.38(4)	Mo4−O35	2.17(4)
Dy1−O40	2.44(3)	Mo4−O17	2.24(4)
Dy1−O18	2.45(3)	Mo4−O27	2.45(4)
Dy1−O28	2.48(3)	$\sum V_{Mo4}^{6+}$	5.78
Dy1−O37	2.54(4)		
Dy1−O11	2.59(3)	Mo5−O5	1.67(3)
$\sum V_{Dy1}^{3+}$	2.95	Mo5−O24	1.75(4)
		Mo5−O6	1.83(4)
Dy2−O21	2.31(4)	Mo5−O35	1.93(3)
Dy2−O5	2.32(4)	Mo5−O4	2.32(5)
Dy2−O46	2.34(3)	Mo5−O22	2.34(3)
Dy2−O20	2.38(4)	$\sum V_{Mo5}^{6+}$	6.23
Dy2−O9	2.40(4)		
Dy2−O12	2.48(5)	Mo6−O41	1.69(3)
Dy2−O30	2.50(3)	Mo6−O18	1.74(4)
Dy2−O8	2.50(4)	Mo6−O33	1.86(6)
Dy2−O31	2.55(4)	Mo6−O43	1.93(5)
$\sum V_{Dy2}^{3+}$	2.98	Mo6−O35	2.14(4)
		Mo6−O17	2.42(3)
Mo1−O42	1.69(4)	$\sum V_{Mo6}^{6+}$	6.23
Mo1−O11	1.78(3)		
Mo1−O43	1.83(4)	Mo7−O2	1.69(5)
Mo1−O16	1.95(4)	Mo7−O9	1.78(4)
Mo1−O27	2.14(4)	Mo7−O26	1.89(4)
Mo1−O17	2.51(4)	Mo7−O6	1.92(4)
$\sum V_{Mo1}^{6+}$	6.06	Mo7−O10	2.02(4)
		Mo7−O22	2.25(4)
Mo2−O44	1.67(4)	$\sum V_{Mo7}^{6+}$	6.35
Mo2−O27	1.84(3)		
Mo2−O4	1.88(4)	Mo8−O29	1.67(4)
Mo2−O10	1.88(4)	Mo8−O37	1.75(4)
Mo2−O25	2.00(4)	Mo8−O16	1.90(4)
Mo2−O22	2.52(4)	Mo8−O25	1.97(4)
$\sum V_{Mo2}^{6+}$	6.17	Mo8−O27	2.19(3)
		Mo8−O36	2.20 (6)
Mo3−O15	1.72(5)	$\sum V_{Mo8}^{6+}$	6.21
Mo3−O46	1.80(4)		
Mo3−O26	1.83(6)		
Mo3−O33	1.94(6)		
Mo3−O25	2.04(4)		
Mo3−O10	2.40(4)		
$\sum V_{Mo3}^{6+}$	6.10		

(27) Mialane, P.; Lisnard, L.; Mallard, A.; Marrot, J.; Antic-Fidancev, E.; Aschehoug, P.; Vivien, D.; Secheresse, F. *Inorg. Chem.* **2003**, *42*, 2102.

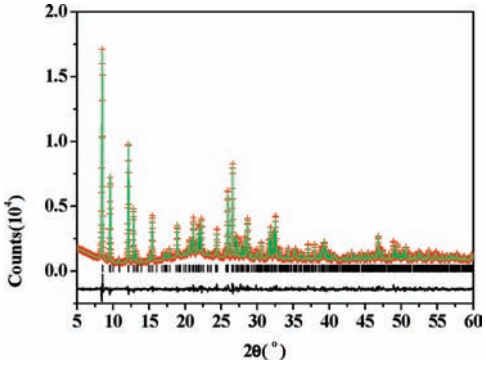

Figure 2. Rietveld plot of the room temperature XRD data for $[Dy_2(H_2O)_{12}](Mo_8O_{27})\cdot 8H_2O$. The ticks mark the Bragg reflection positions.

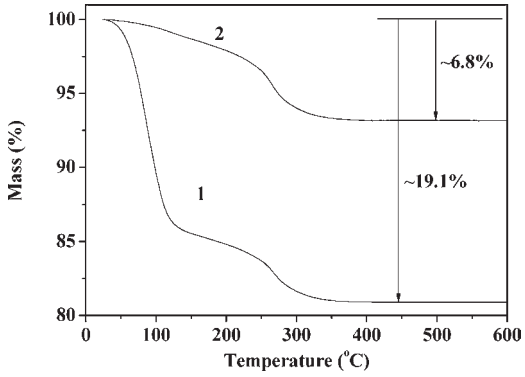

Figure 3. TGA data for $[Dy_2(H_2O)_{12}](Mo_8O_{27})\cdot 8H_2O$ (1) and $[Dy_2(H_2O)_6]Mo_8O_{27}$ (2).

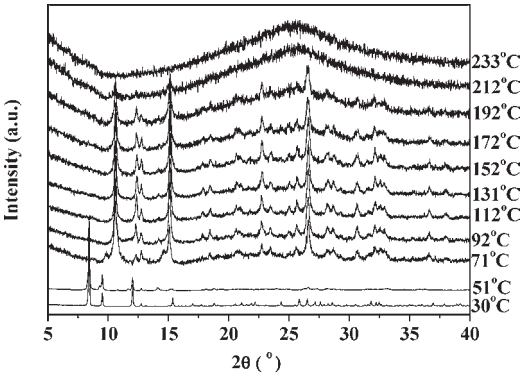

Figure 4. VT XRD data for $[Dy_2(H_2O)_{12}](Mo_8O_{27})\cdot 8H_2O$ in the range 30−233 °C, showing the partial dehydration leading to a new crystalline phase stable from 70 to 200 °C.

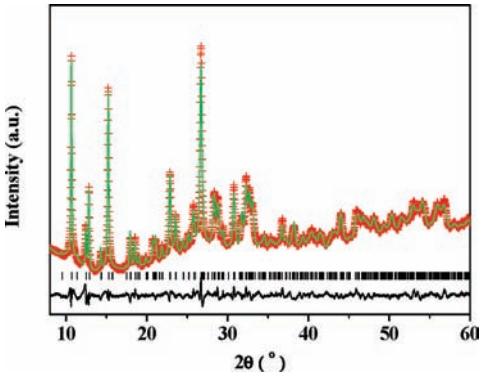

Figure 5. Rietveld fit obtained for the room temperature XRD pattern of $[Dy_2(H_2O)_6](Mo_8O_{27})$. The ticks mark the Bragg reflection positions.

Topotactic Dehydration of $[Dy_2(H_2O)_{12}](Mo_8O_{27})\cdot 8H_2O$ into $[Dy_2(H_2O)_6](Mo_8O_{27})$. The TGA data in Figure 3 (curve 1) show that $[Dy_2(H_2O)_{12}](Mo_8O_{27})\cdot 8H_2O$ undegoes a sharp dehydration below 100 °C and a more gradual, further dehydration in the range 100−250 °C, suggesting a phase transformation, before reaching a constant weight at ~350 °C. The VT XRD data in Figure 4 show that the dehydration results in the formation of a new phase stable from 70 to 200 °C, in agreement with the mass plateau in the 100−250 °C range in the TGA data. This new phase can be reproducibly prepared in bulk quantities by heating the $[Dy_2(H_2O)_{12}](Mo_8O_{27})\cdot 8H_2O$ precursor at 100 °C for 3 h. The water content in the partially dehydrated material, derived from the TGA data (Figure 3, curve 2), is 6.2(2) per $Dy_2Mo_8O_{27}$.

The XRD reflections of the partially dehydrated product $[Dy_2(H_2O)_6](Mo_8O_{27})$ can be indexed using a monoclinic cell: a = 14.1242(5) Å, b = 10.1306(4)Å, c = 9.2984(5)Å, and β = 89.853(5)° with space group $P2_1$ (consistent with systematic absences and a positive SHG test). The b axis and the c axis for $[Dy_2(H_2O)_6](Mo_8O_{27})$ are almost identical to those in $[Dy_2(H_2O)_{12}](Mo_8O_{27})\cdot 8H_2O$, while the a axis is reduced by about one-third (6.6 Å) relative to the precursor (see Table 1). This implies that the condensation of the structural building blocks after dehydration occurs principally along the a axis. Thus, an initial structure model for the Rietveld analysis of the new $[Dy_2(H_2O)_6](Mo_8O_{27})$ structure was derived from the structure of the $[Dy_2(H_2O)_{12}](Mo_8O_{27})\cdot 8H_2O$ precursor. The refinement converged to R_p = 1.08% and R_{wp} = 1.52%, and the Rietveld refinement plot for $[Dy_2(H_2O)_6](Mo_8O_{27})$ is shown in Figure 5. The final refined structural parameters are listed in Table S2 (Supporting Information), while the bond lengths and bond valence sums are given in Table 3.

Two views of the $[Dy_2(H_2O)_6](Mo_8O_{27})$ structure are shown in Figure 1c,d. A comparison with the structure of the precursor (Figure 1a,b) suggests that this partial dehydration is a topotactic transformation. The zigzag-type assembly of $Dy_2Mo_8O_{27}$ units is retained, and the structure is condensed by the removal of crystallized water molecules, which, in the precursor, lie between the $(Dy_2Mo_8O_{27})_n$ polymeric sheets running along the c axis.

The topotactic nature of this transformation is more easily understood using the schematic representations in Figure 6. The two views given for $[Dy_2(H_2O)_{12}](Mo_8O_{27})\cdot 8H_2O$ (Figure 6a,b) and $[Dy_2(H_2O)_6](Mo_8O_{27})$ (Figure 6c,d) correspond to the crystal structure projections shown in Figure 1. In these schematics, the "Dy_2Mo_2" polygons represent $(Dy_2Mo_8O_{27})_n$ building blocks, which are isolated in the precursor, in the sense that they form chains, without three-dimensional cross-linking. Upon partial dehydration, each Dy atom within these $Dy_2Mo_8O_{27}$ units bridges two adjacent $(Mo_8O_{27})^{6-}$ chains to form a 3D-linked framework. The coordination number of Dy is reduced from 9 in the precursor to 8 in $[Dy_2(H_2O)_6](Mo_8O_{27})$: each Dy atom bonds to three oxygen atoms from the neighboring Mo_8O_{27} units, two oxygen atoms from the next nearest $(Mo_8O_{27})^{6-}$ chain, and three oxygen atoms from crystallized water. Lanthanide-bridged units

Table 3. Bond Lengths and Bond Valence Sums of Dy^{3+} and Mo^{6+} in $[Dy_2(H_2O)_6](Mo_8O_{27})$

bond	bond length (Å)	bond	bond length (Å)
Dy1−O6	2.22(3)	Mo4−O8	1.72(4)
Dy1−O30	2.39(4)	Mo4−O9	1.73(3)
Dy1−O33	2.39(3)	Mo4−O17	1.75(4)
Dy1−O14	2.42(3)	Mo4−O5	2.12(3)
Dy1−O17	2.42(3)	Mo4−O16	2.38(3)
Dy1−O18	2.44(3)	Mo4−O13	2.51(3)
Dy1−O28	2.46(4)	$\sum V_{Mo4}^{6+}$	5.84
Dy1−O2	2.50(3)		
$\sum V_{Dy1}^{3+}$	2.75	Mo5−O10	1.67(3)
		Mo5−O25	1.72(3)
Dy2−O24	2.34(3)	Mo5−O8	1.83(3)
Dy2−O19	2.36(2)	Mo5−O16	2.18(3)
Dy2−O25	2.38(3)	Mo5−O26	2.35(4)
Dy2−O29	2.39(4)	Mo5−O19	2.48(3)
Dy2−O32	2.39(4)	$\sum V_{Mo5}^{6+}$	5.78
Dy2−O31	2.47(4)		
Dy2−O27	2.48(3)	Mo6−O6	1.73(3)
Dy2−O10	2.51(3)	Mo6−O20	1.74(3)
$\sum V_{Dy2}^{3+}$	2.65	Mo6−O16	1.79(3)
		Mo6−O15	1.99(4)
Mo1−O2	1.71(3)	Mo6−O22	2.21(5)
Mo1−O21	1.75(3)	Mo6−O5	2.27(3)
Mo1−O22	2.00(4)	$\sum V_{Mo6}^{6+}$	6.17
Mo1−O4	2.00(4)		
Mo1−O13	2.13(3)	Mo7−O7	1.70(3)
Mo1−O5	2.39(4)	Mo7−O27	1.73(3)
$\sum V_{Mo1}^{6+}$	5.61	Mo7−O26	1.91(4)
		Mo7−O12	1.95(4)
Mo2−O23	1.65(3)	Mo7−O1	2.48(3)
Mo2−O19	1.71(3)	Mo7−O8	2.52(3)
Mo2−O13	1.91(3)	$\sum V_{Mo7}^{6+}$	5.65
Mo2−O11	2.15(3)		
Mo2−O1	2.38(3)	Mo8−O14	1.69(3)
Mo2−O8	2.49(3)	Mo8−O18	1.70(3)
$\sum V_{Mo2}^{6+}$	5.70	Mo8−O11	1.99(3)
		Mo8−O4	2.00(4)
Mo3−O3	1.73(2)	Mo8−O13	2.39(3)
Mo3−O24	1.75(3)	Mo8−O17	2.50(4)
Mo3−O15	1.84(4)	$\sum V_{Mo8}^{6+}$	5.60
Mo3−O12	1.96(4)		
Mo3−O11	2.14(3)		
Mo3−O1	2.43(3)		
$\sum V_{Mo3}^{6+}$	5.98		

forming 3D frameworks have been observed in a few polyoxometalates.[28,29] Similarly to the precursor, $[Dy_2(H_2O)_6](Mo_8O_{27})$ exhibits an SHG efficiency 5 times that of α-SiO_2, demonstrating that the topotactic partial dehydration has no detrimental effect on the second-order nonlinear optical properties.

$[Nd_2(H_2O)_{12}](Mo_8O_{27})\cdot 6H_2O$ and partial dehydration to $[Nd_2(H_2O)_{12}](Mo_8O_{27})\cdot 6H_2O$. $[Nd_2(H_2O)_{12}](Mo_8O_{27})\cdot 6H_2O$ is isostructural with $[Eu_2(H_2O)_{12}](Mo_8O_{27})\cdot 6H_2O$,[15] and this structure was used as the starting model for the Rietveld analysis. Two views of the $[Nd_2(H_2O)_{12}](Mo_8O_{27})\cdot 6H_2O$ crystal structure are shown in Figure 7a,b and the Rietveld refinement plot (R_p = 2.66% and R_{wp} = 3.96%) in Figure 8. The refined structural parameters are given in Table S3 (Supporting Information) and bond lengths in Table 4.

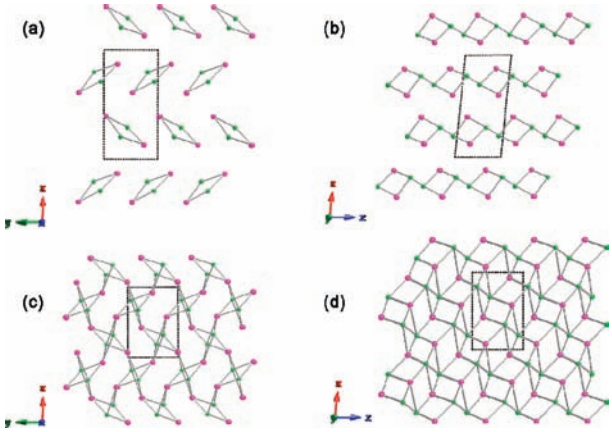

Figure 6. Schematic representations of topologies of $[Dy_2(H_2O)_{12}](Mo_8O_{27})\cdot 8H_2O$, (a) along [001] and (b) along [010], and $[Dy_2(H_2O)_6](Mo_8O_{27})$, (c) along [001] and (d) along [010]. Pink spheres represent Dy; green spheres represent Mo. Each "Dy_2Mo_2" unit represents a $Dy_2Mo_8O_{27}$ sheet running along the *z* axis.

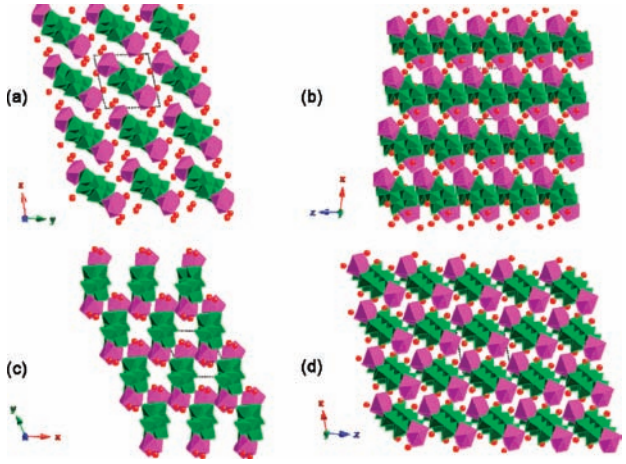

Figure 7. Two views of the crystal structure of $[Nd_2(H_2O)_{12}](Mo_8O_{27})\cdot 6H_2O$, (a) along [001] and (b) along [010], and the crystal structure of the partially dehydrated product $[Nd_2(H_2O)_6]Mo_8O_{27}\cdot 3H_2O$, (c) along [001] and (d) along [010]. The red spheres represent the water oxygen atoms not coordinated to Nd (in pink polyhedra); MoO_6 octahedra are shown in green.

TGA data in Figure 9 (curve 1) show that $[Nd_2(H_2O)_{12}](Mo_8O_{27})\cdot 6H_2O$ undergoes a gradual dehydration with increasing temperature up to ~350 °C to reach a constant mass. The VT powder XRD data (Figure 10) show that the dehydration initially results in the formation of a new crystalline phase, stable in a narrow temperature region between 50 and 100 °C.

This new material can also be prepared as a bulk phase by heating the $[Nd_2(H_2O)_{12}](Mo_8O_{27})\cdot 6H_2O$ precursor at 80 °C for 3−4.5 h. The water content in the new phase can vary from 6 to 12 (according to TGA), depending on the dwelling time and initial precursor mass used. XRD data for the ab initio structure solution of the new partially dehydrated material were collected on a sample which was prepared by heating ~0.3 g of $[Nd_2(H_2O)_{12}](Mo_8O_{27})\cdot 6H_2O$ at 80 °C for 4.5 h. The TGA data showed that this sample contains 8.7(1) water per $Nd_2Mo_8O_{27}$ (Figure 9, curve 2), which we describe using a nominal composition of $[Nd_2(H_2O)_6]Mo_8O_{27}\cdot 3H_2O$.

The XRD reflections of the partially dehydrated $[Nd_2(H_2O)_6]Mo_8O_{27}\cdot 3H_2O$ can be indexed using a triclinic

(28) Zhang, X. T.; Wang, D. Q.; Dou, J. M.; Yan, S. S.; Yao, X. X.; Jiang, J. Z. *Inorg. Chem.* **2006**, *45*, 10629.
(29) Wu, C. D.; Lu, C. Z.; Zhuang, H. H.; Huang, J. S. *J. Am. Chem. Soc.* **2002**, *124*, 3836.
(30) Leisegang, T.; Levin, A. A.; Walter, J.; Meyer, D. C. *Cryst. Res. Technol.* **2005**, *40*, 95.
(31) Efremov, V. A.; Davydova, N. N.; Gokhman, L. Z.; Evdokimov, A. A.; Trunov, V. K. *Zh. Neorg. Khim.* **1988**, *33*, 3005.
(32) Jeitschko, W. *Acta Crystallogr., Sect. B* **1973**, *29*, 2074.

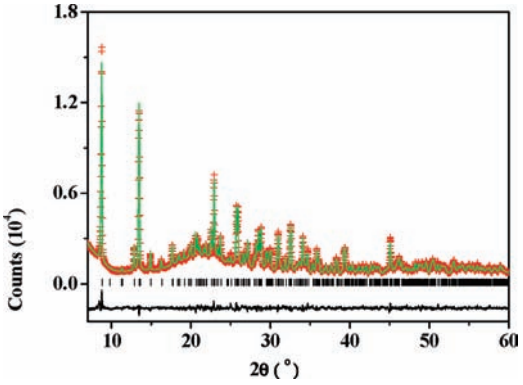

Figure 8. Rietveld fit of the XRD pattern of $[Nd_2(H_2O)_{12}](Mo_8O_{27})\cdot 6H_2O$. The ticks mark the Bragg reflection positions.

cell: $P\bar{1}$, $a = 8.9912(6)$ Å, $b = 10.3378(6)$ Å, $c = 9.2850(5)$ Å, $\alpha = 112.840(5)°$, $\beta = 91.518(5)°$, and $\gamma = 111.760(4)°$. The crystal structure of $[Nd_2(H_2O)_6]Mo_8O_{27}\cdot 3H_2O$ is shown in Figure 7c,d. The final refined structural parameters are listed in Table S4 (Supporting Information), the bond lengths and bond valence sums in Table 5, and the Rietveld refinement plot of XRD data for $[Nd_2(H_2O)_6]Mo_8O_{27}\cdot 3H_2O$ is shown in Figure 11. The asymmetric unit contains one Nd, four Mo, and 19 O atoms. Water oxygen atoms are located on five of these oxygen sites (O1, O2, O14, O15, and O16 in Table S4, Supporting Information). In our structural model, we propose that three of these oxygen sites which bond to the Nd cations only (O14, O15, and O16) are fully occupied (to give rise to an 8-fold coordination for Nd). The fractional occupancies of O1 and O2 sites (which do not bond to Nd or Mo) were fixed to 0.75, leading to the nominal composition $[Nd_2(H_2O)_6]Mo_8O_{27}\cdot 3H_2O$. This gives a plausible and chemically sensible model; it should, however, be noted that it is not possible to determine accurately the occupancies and the distribution of the water oxygen atoms in $[Nd_2(H_2O)_6]Mo_8O_{27}\cdot 3H_2O$ from our XRD data.

The topotactic tranformation of $[Nd_2(H_2O)_{12}](Mo_8O_{27})\cdot 6H_2O$ into $[Nd_2(H_2O)_6]Mo_8O_{27}\cdot 3H_2O$ is represented schematically in Figure 12.

The initial topology in $[Nd_2(H_2O)_{12}](Mo_8O_{27})\cdot 6H_2O$ is very similar to that in $[Dy_2(H_2O)_{12}](Mo_8O_{27})\cdot 8H_2O$, the main difference being the parallel (as opposed to zigzag or herringbone) packing of the $Nd_2Mo_8O_{27}$ sheets (Figures 7a and 12a). Topotactic dehydration of $[Nd_2(H_2O)_{12}](Mo_8O_{27})\cdot 6H_2O$ and the relationship between the precursor and the product can be understood by transforming the primitive cells to larger C-centered cells for both phases. The transformation matrices are

$$\begin{bmatrix} 1 & 1 & 0 \\ -1 & 1 & 0 \\ 0 & 0 & 1 \end{bmatrix}$$

and

$$\begin{bmatrix} 1 & 0 & 0 \\ 1 & 2 & 0 \\ 0 & 0 & 1 \end{bmatrix}$$

Table 4. Bond Lengths and Bond Valences of Nd^{3+} and Mo^{6+} in $[Nd_2(H_2O)_{12}](Mo_8O_{27})\cdot 6H_2O$

bond	bond length (Å)	bond	bond length (Å)
Nd−O15	2.41(2)	Mo3−O14	1.71(2)
Nd−O17	2.44(2)	Mo3−O1	1.77(2)
Nd−O21	2.45(2)	Mo3−O6	1.87(1)
Nd−O1	2.47(2)	Mo3−O2	2.08(2)
Nd−O16	2.48(2)	Mo3−O4	2.11(1)
Nd−O11	2.49(2)	Mo3−O8	2.38(2)
Nd−O7	2.52(2)	$\sum V_{Mo3}^{6+}$	5.74
Nd−O19	2.56(2)		
Nd−O18	2.68(3)	Mo4−O11	1.72(2)
$\sum V_{Nd}^{3+}$	3.16	Mo4−O10	1.77(1)
		Mo4−O5	1.898(6)
Mo1−O4	1.73(2)	Mo4−O6	1.95(2)
Mo1−O7	1.75(2)	Mo4−O3	2.03(2)
Mo1−O9	1.77(1)	Mo4−O8	2.38(1)
Mo1−O3	2.07(3)	$\sum V_{Mo4}^{6+}$	6.02
Mo1−O2	2.27(1)		
Mo1−O12	2.37(2)		
$\sum V_{Mo1}^{6+}$	5.89		
Mo2−O13	1.69(2)		
Mo2−O12	1.74(1)		
Mo2−O8	1.88(2)		
Mo2−O2	1.98(2)		
Mo2−O3	2.03(1)		
Mo2−O2	2.44(2)		
$\sum V_{Mo2}^{6+}$	6.22		

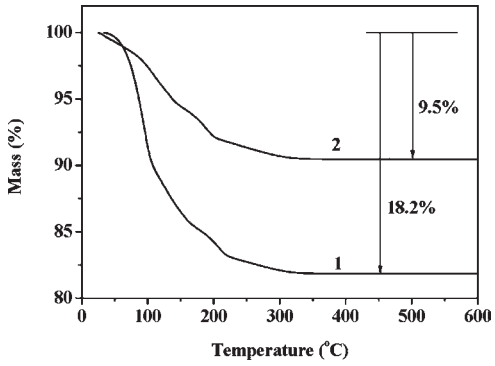

Figure 9. TGA data of $[Nd_2(H_2O)_{12}](Mo_8O_{27})\cdot 6H_2O$ (1) and $[Nd_2(H_2O)_6]Mo_8O_{27}\cdot 3H_2O$ (2).

for the fully hydrated precursor and the partial dehydration product, respectively. The [110] axis and $[1\bar{1}0]$ axis in the precursor structure (Figure 7a,b) hence correspond to the *a* axis and [120] axis in the product (Figure 7c,d), respectively. The partial dehydration condenses the structure $[Nd_2(H_2O)_{12}](Mo_8O_{27})\cdot 6H_2O$ along the [110] axis, which contracts by ~30% from ~14.6 Å to ~9 Å. The [120] axis expands by ~15%, from ~16.8 Å to ~19.2 Å, to accommodate the formation of new linkages between $Nd_2Mo_8O_{27}$ units as a consequence of the condensation along the [110] axis. These changes lead to mutual shifting of the $Nd_2Mo_8O_{27}$ sheets (at different levels on the [110] axis) along the [001] direction (Figure 7b and d). Partial dehydration and the condensation of the crystal structure result in linking each Nd^{3+} to three $(Mo_8O_{27})^{6-}$ sheets and give rise to three-dimensional connectivity and a framework with channels along the *c* axis (Figure 7c). The Nd coordination number is consequently reduced from 9 in the precursor to 8 in $[Nd_2(H_2O)_6]Mo_8O_{27}\cdot 3H_2O$, with the coordination sphere formed by five oxygen atoms belonging to neighboring

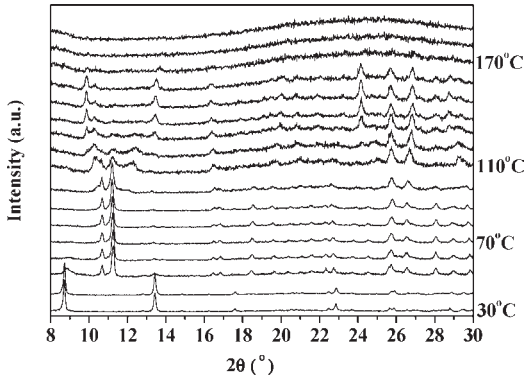

Figure 10. VT XRD data of $[Nd_2(H_2O)_{12}](Mo_8O_{27})\cdot 6H_2O$ within 30−200 °C, showing the partial dehydration resulting in a new crystalline phase stable between 50 and 100 °C.

Table 5. Bond Lengths and Bond Valence Sums of Nd^{3+} and Mo^{6+} in $[Nd_2(H_2O)_6](Mo_8O_{27}))\cdot 3H_2O$

bond	bond length (Å)	bond	bond length (Å)
Nd−O14	2.40(2)	Mo3−O18	1.72(2)
Nd−O18	2.43(2)	Mo3−O17	1.73(2)
Nd−O17	2.44(2)	Mo3−O11	1.98(2)
Nd−O8	2.46(2)	Mo3−O7	2.00(2)
Nd−O15	2.46(2)	Mo3−O6	2.04(2)
Nd−O16	2.47(2)	Mo3−O4	2.37(2)
Nd−O12	2.47(2)	$\sum V_{Mo3}^{6+}$	5.85
Nd−O19	2.49(2)		
$\sum V_{Nd}^{3+}$	3.14	Mo4−O12	1.66(2)
		Mo4−O19	1.81(2)
Mo1−O8	1.65(2)	Mo4−O6	1.84(2)
Mo1−O5	1.76(3)	Mo4−O13	1.90(2)
Mo1−O10	1.938(6)	Mo4−O7	2.12(2)
Mo1−O13	2.00(3)	Mo4−O9	2.48(1)
Mo1−O11	2.06(2)	$\sum V_{Mo4}^{6+}$	6.24
Mo1−O9	2.38(2)		
$\sum V_{Mo1}^{6+}$	6.13		
Mo2−O3	1.77(2)		
Mo2−O4	1.79(2)		
Mo2−O9	1.84(2)		
Mo2−O7	1.92(3)		
Mo2−O11	2.25(2)		
Mo2−O7	2.36(2)		
$\sum V_{Mo2}^{6+}$	5.67		

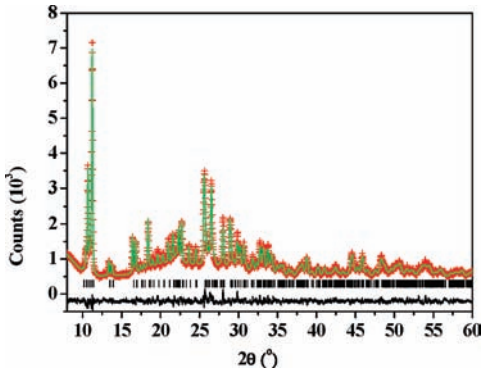

Figure 11. Rietveld refinement of ambient temperature XRD data for partially dehydrated $[Nd_2(H_2O)_6]Mo_8O_{27}\cdot 3H_2O$. The ticks mark the Bragg reflection positions.

Mo_8O_{27} units and three oxygen atoms from crystallized water.

The existence of three remaining crystallized water molecules outside the 3D-framework in $[Nd_2(H_2O)_6]$-$Mo_8O_{27}\cdot 3H_2O$ suggests that further dehydration to

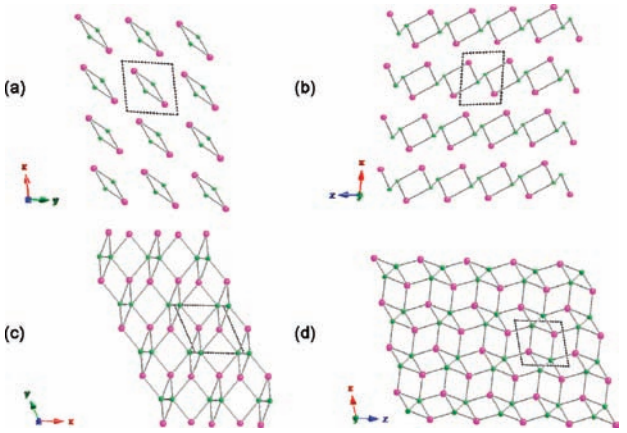

Figure 12. Schematic representations of topologies of $[Nd_2(H_2O)_{12}]$-$(Mo_8O_{27})\cdot 6H_2O$, (a) along [001] and (b) along [010], and $[Nd_2(H_2O)_6]$-$Mo_8O_{27}\cdot 3H_2O$, (c) along [001] and (d) along [010]. Pink spheres represent Nd; green spheres represent Mo. Each "Nd_2Mo_2" unit represents a $Nd_2Mo_8O_{27}$ sheet running along the *z* axis.

$[Nd_2(H_2O)_6]Mo_8O_{27}$ with the framework maintained is possible, as we have established in the case of $[Dy_2$-$(H_2O)_6]Mo_8O_{27}$. This is consistent with a water content lower than nine per formula unit, which we observed from TGA experiments on different partially dehydrated samples, as described above.

On further heating, both Dy and Nd hydrated frameworks collapse before transforming, via an amorphous phase and a number of known mixed oxides, into an unknown crystalline product and $Nd_2Mo_3O_{12}$, respectively. Further details of the high temperature decompositions are given in the Supporting Information.

Conclusions

Two different structure types have been demonstrated for highly hydrated Nd and Dy octamolybdates. Both contain $RE_2Mo_8O_{27}$ sheets as the basic building blocks, and the packing arrangement of these sheets dictates the final structure type adopted. $[Nd_2(H_2O)_{12}]Mo_8O_{27}\cdot 6H_2O$, isostructural with the known Eu ad Sm analogues, crystallizes in space group $P\bar{1}$ with a parallel arrangement of the $RE_2Mo_8O_{27}$ sheets, which is preserved during topotactic partial dehydration into $[Nd_2(H_2O)_6]Mo_8O_{27}\cdot 3H_2O$. $[Dy_2$ $(H_2O)_{12}]$-$(Mo_8O_{27})\cdot 8H_2O$ is SHG active, and it crystallizes in a new structure type, in noncentrosymmetric polar space group $P2_1$, with zigzag (or herringbone) packing of the $RE_2Mo_8O_{27}$ sheets. Again, this packing motif, the space group, and the SHG activity of the highly hydrated Dy phase are preserved upon topotactic dehydration into $[Dy_2(H_2O)_6]Mo_8O_{27}$.

Different packing motifs of the $RE_2Mo_8O_{27}$ sheets in the polar Dy octamolybdates and the centrosymmetric Nd, Sm, and Eu octamolybdates demonstrate the dependency of the assembly of polyoxometalate building blocks on the nature of the rare-earth cation. The condensation of $RE_2Mo_8O_{27}$ sheets to form 3D-linked frameworks upon partial dehydration demonstrates water-content-dependent dimensionality control in polyoxometalates and an effective way to topotactially prepare new polyoxometalate materials.

Acknowledgment. The authors thank the EPSRC for funding though grant EP/F030371, Douglas Carswell for

assistance with the TGA experiments, and Jeongho Yeon and Shiv Halasyamani for the SHG measurements.

Supporting Information Available: Final refined atomic positions of $[Dy_2(H_2O)_{12}](Mo_8O_{27})\cdot 8H_2O$, $[Dy_2(H_2O)_6](Mo_8O_{27})$, $[Nd_2(H_2O)_{12}](Mo_8O_{27})\cdot 6H_2O$, and $[Nd_2(H_2O)_6]Mo_8O_{27}\cdot 3H_2O$; description of high temperature decomposition; and selected multiphase Rietveld refinement plots of VT XRD data for dysprosium and neodymium octamolybdates. This material is available free of charge via the Internet at http://pubs.acs.org.